ILASS–Europe 2017, 28th Conference on Liquid Atomization and Spray Systems, 6-8 September 2017, Valencia, Spain
http://dx.doi.org/10.4995/ILASS2017.2017.5001

Characterization of Liquid Impinging Jet Injector Sprays for Bi-Propellant Space Propulsion: Comparison of PDI and High-Magnification Shadowgraphy

Bastien Boust*[1], Quentin Michalski[1], Alain Claverie[1], Clément Indiana[1], Marc Bellenoue[1]
[1]Institut PPRIME, CNRS/ISAE-ENSMA/Université de Poitiers, France
*Corresponding author: bastien.boust@ensma.fr

Abstract
Impinging jet sprays are investigated in the reference case of like-doublet injector, for application to bi-propellant combustion. Green propellants are considered, namely ethanol as a fuel and hydrogen peroxide as an oxidizer, that is well represented by water. This study reports original comparisons between standard spray characterization (PDI) and high-magnification shadowgraphy of the spray (2.5 x 3.2 mm, 2.5 µm per pixel) based on short laser backlight illumination (5 ns). Shadowgraphy images describe accurately the inner spray structure and provide the size and velocity of droplets. This diagnostic is used to analyse the influence of jet momentum (driven by injection pressure) on impinging jet atomization, as well as the evolution of spray topology, drop size distribution and average diameter along the spray centreline. The application of shadowgraphy to the dense region of water and ethanol sprays shows the different atomization behaviour of these two fluids with respect to their surface tension. Elliptical droplets are characterized inside the spray, which confirms the interest of a direct visualization of droplets in such dense sprays.

Keywords
Liquid impinging jet injector, Atomization, Shadowgraphy, Droplet sizing.

Introduction

Impinging jet injectors are used in most storable bi-propellant space engines. Current storable propellants such as hydrazine and nitrogen tetroxide usually burn after hypergolic ignition, which is allowed by their chemical properties. However, these toxic propellants are to be replaced by “green” propellants, e.g. hydrogen peroxide and ethanol, which atomization, ignition and combustion deserve additional knowledge. Particularly, compared to current storable propellants, the atomization of green propellants may be less prone: i. to generate small droplets due to their surface tension, ii. to generate a gaseous phase to their low volatility (e.g. hydrogen peroxide), iii. to ignite and burn efficiently, as a result. Therefore, attention must be paid to the atomization process of these new “green” propellants, particularly in the physical conditions encountered in combustion chambers i.e. subcritical at high temperature and pressure.

In practice, liquid propellants atomization is usually based on jet impingement, which is a common way to generate droplets with moderate levels of pressure (e.g. a few MPa). In this study, the like-doublet configuration is considered as a reference case, even though real engines injectors may also feature unlike jet impingement (e.g. fuel on oxidizer) such as doublets or triplets etc. In the literature, numerous studies already address this like-doublet configuration in the spraying regime related to engine conditions, i.e. at elevated Reynolds and Weber numbers (10^3–10^4) leading to ligaments and fully developed breakup; a review of such spray phenomena can be drawn from detailed experiments [1]. Like-impinging doublets are investigated through theoretical studies [2] and numerical simulation [3]-[4], highlighting the dynamics of the liquid sheet breakup that generates wavy ligaments and then droplets. However in this complex situation, the reference knowledge concerning the spray shape, the distribution of droplet size and velocity, is provided by experiments [5]-[8]; for this purpose, most studies are based on Phase-Doppler Interferometer (PDI) and direct visualization of the spray. In these fundamental experiments the droplet distribution is well characterized downstream the dense part of the spray (i.e. downstream the liquid sheet), but in real engine conditions the flame affects the spray even from the dense zone [8], so that the spray properties cannot be inferred directly from inert condition measurements. This makes spray combustion all the more complex because drop size influences combustion performance and induction length, as an example. Moreover, the Sauter Mean Diameter (SMD) measured with PDI is found to increase with increasing distance from the impingement point [5]-[6], whereas it is found to decrease in another study combining experiment and simulation [3]. This contradiction shows that impinging jet sprays deserve a specific study, in order to discuss the methods used to analyse the structure of such sprays.

EDITORIAL UNIVERSITAT POLITÈCNICA DE VALÈNCIA

Thus, the specific objective of this work is to perform original comparisons between standard spray characterization based on PDI, and high-magnification shadowgraphy of the spray. This last diagnostic is known to provide better results in dense sprays [9]. Thanks to this diagnostic, a direct analysis of the spray structure is expected and may provide additional information to the classical PDI analysis. The influence of jet velocity is investigated through the influence of injection pressure, as well as the effect of fluid properties (water or ethanol), for elevated Reynolds and Weber numbers (10^3–10^4) leading to a “ligament-structure” or “fully-developed” spray.

Experiment and diagnostics

Experimental apparatus

The liquids of interest are sprayed using a classical setup for impinging jets under inert gas pressurization, as described in former studies [2],[5]. The two jets of the like-doublet are generated from 2 symmetrical orifices manufactured in a single stainless steel injector designed for combustion experiments; they are drilled with a diameter d_0 = 0.3 mm, a length L/d_0 = 20, and an angle of impingement 60°, that provides good momentum while preventing from backsplash and erosion of the injector. The velocity of the jets is governed by the pressure drop ΔP across the injector through Bernoulli equation: $V = \sqrt{2\,\Delta P/\rho}$.

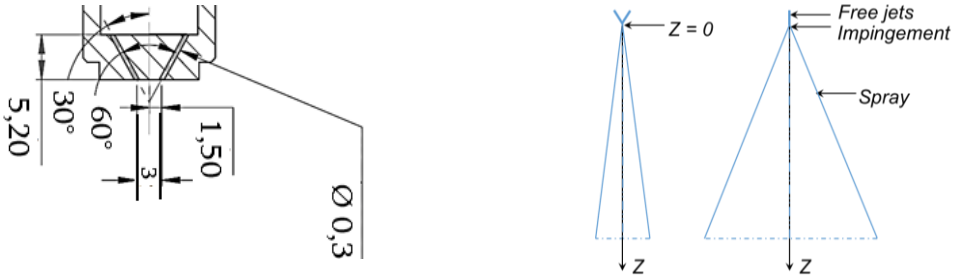

Figure 1. Experimental injector geometry.

The study focuses on green storable propellants, such as ethanol and hydrogen peroxide. Spraying conditions are characterized by the Reynolds (1), Weber (2) and Ohnesorge (3) dimensionless numbers. For safety purposes, deionized water is used to represent the atomization behaviour of hydrogen peroxide, since they have similar *We* and *Oh* numbers (see Table 1). In this table, High Test Peroxide (HTP) of mass concentration 87.5% is reported but not used experimentally. According to the behaviour of impinging jet sprays [1], the magnitude of *Re* and *We* numbers settle our experiments in the “ligament-structure” or “fully-developed” atomization regimes. For this purpose, the relevant injection conditions are reached by controlling the jet momentum thanks to the pressure drop across the injector ΔP = 0.9–3.0 MPa.

$$\mathrm{Re} = \frac{\sqrt{2\rho\Delta P}\times d_0}{\mu} \tag{1}$$

$$We = \frac{2\Delta P\times d_0}{\sigma} \tag{2}$$

$$Oh = We^{1/2}\,\mathrm{Re}^{-1} = \frac{\mu}{\sqrt{\rho\sigma d_0}} \tag{3}$$

Table 1. Fluid properties and experimental conditions for d_0 = 0.30 mm – HTP is not used experimentally.

	Water		Ethanol		HTP	
Density ρ (kg/m3)	998		792		1379	
Surface tension σ (N/m)	0.073		0.022		0.079	
Dynamic viscosity μ (kg/m/s)	1.002 E-3		1.272 E-3		1.260 E-3	
Oh	0.006 78		0.017 59		0.006 98	
ΔP (MPa)	*Re*	*We*	*Re*	*We*	*Re*	*We*
0.9	12 690	7 400	8 900	24 550	11 860	6 840
1.5	16 380	12 330	11 500	40 910	15 310	11 400
3.0	23 170	24 660	16 260	81 820	21 660	22 790

Spray analysis based on Phase-Doppler Interferometer

Following the initial development of Bachalo, the Phase-Doppler Interferometer (PDI) has proved to stand as a powerful standard laser-based diagnostic instrument for simultaneous and accurate measurements of the size and velocity of individual spherical particles in polydisperse particle flow environment [2],[5]-[6].

A modular PDI system (Artium 200 MD) is used for the real-time, non-intrusive measurement of individual drop size and 2 velocity components in this application. The diode-pumped solid-state lasers used in the transmitter provide 532 nm and 473 nm wavelengths. The distances from transmitter to probe volume, and from receiver to probe volume, are set to 500 mm allowing 4.33 µm fringe spacing and a range of diameters between 1.5 µm and 160 µm when used with a light scattering angle set to 40°. The probe volume dimensions are characterized by a quasi-circular cross-section of diameter 0.34 mm, and a length of 5.6 mm. PDI data processing includes the classical "probe-volume correction" (PVC) that compensates for the effect of varying sample volume on drop size.

Spray analysis based on high-magnification shadowgraphy

High-magnification shadowgraphy is recorded with pulsed backlight illumination, that is independent of the shape and material of the particles (either transparent or opaque) and allows for the investigation of drop size down to a few microns per pixel. Based on a PIV system, this technique is expected to provide information on the droplets shape coupled with size distribution and velocity.

As illustrated (see Figure 2), a double-pulse Nd:YAG laser (Continuum Minilite II, 2*25 mJ/pulse) is combined with a double-frame camera (LaVision Flowmaster 3S, 1280 x 1024 px, 6.35 µm/px) equipped with a long-distance microscope (Questar QM1) of 60 cm working distance. A diffusor optics with a wavelength shifting fluorescing plate is mounted to the laser beam outlet, which yields a homogenous speckle-free backlight illumination of wavelength around 590 nm. The measurement volume is defined by the focal plane and the depth of field of the imaging system. The image size is 2.5 x 3.2 mm, and image pixel size is 2.5 µm. Given a f-number for the optics of 9.3, the effective spatial resolution based on Rayleigh criterion is 5.6 µm. The short laser pulsewidth (between 3 and 5 ns) ensures the motion freezing of all imaged droplets. Conventional corrections are applied to the drop size distributions using statistical weighting functions, in order to compensate for the so-called "border" and "depth-of-field" effects [9].

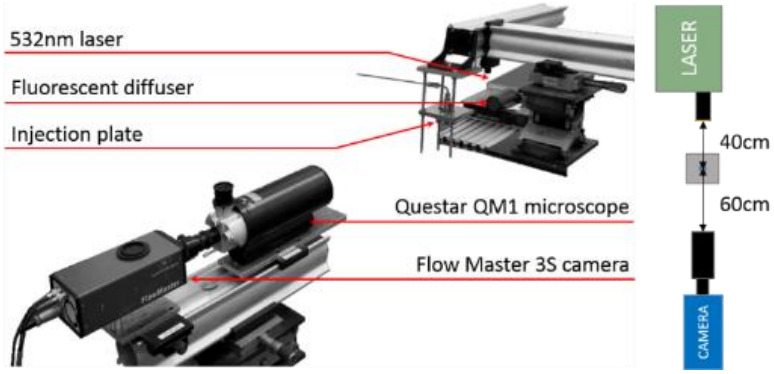

Figure 2. Experimental setup for high-magnification shadowgraphy.

Images are analysed using commercial software (ParticleMaster Shadow, Lavision) that includes several parameters for droplet detection (see Figure 3). The first one is the kernel width of a sliding maximum filter, which is used to ensure background homogeneity for droplets detection prior to the first segmentation: it is set to 100 px (250 µm). The binarisation threshold for the first segmentation is a global threshold relative to the maximum intensity found on the image: it is set to 50%. A second segmentation computes a droplet diameter based on an average between the 40%- and 60%-threshold relative to the local maximum on the droplet. Blurry particles are rejected based on a minimum slope criterion, locally defined as the relative intensity decrease at the particle rim: it is set to 20%. Given the intensity difference between small and large droplets, the admissible depth of field depends on drop size. Based on the slope criterion, it is comprised between 50 µm for the smallest droplets, and 330 µm for the biggest ones. Droplet velocity is computed from each doublet of images, provided the droplet is identified in both frames. The identification is based on a diameter variation inferior to 15%, and to a vertical velocity comprised between –10 and 50 m/s. For each condition, 20 doublets of images are recorded at 2 Hz with 2 µs delay between frames, which yields up to 50 validated droplets per frame.

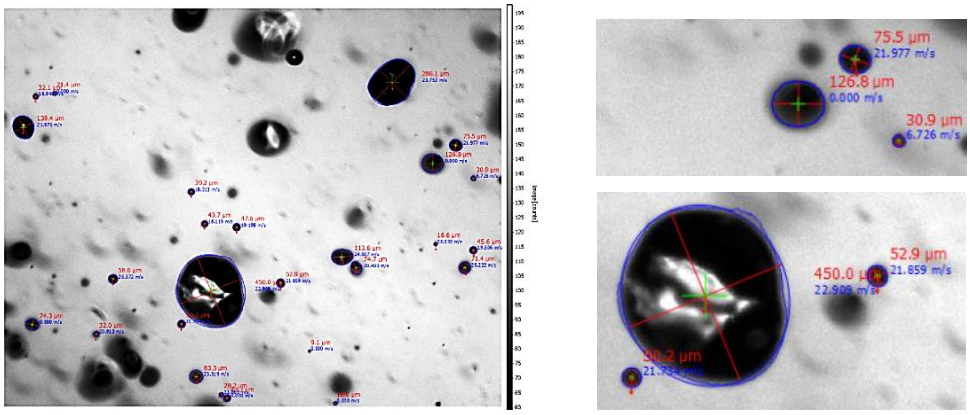

Figure 3. Example of particle detection obtained by the software – Water spray, 0.9 MPa, Z/d_0 = 100.

Even though shadowgraphy is far less sensitive to droplet shape for detection, it may detect overlapping droplets or ligaments to which is attributed an elliptical cross-section (see Figure 4). In order to avoid such erroneous particles, images are computed using a second exclusion criterion, based on the ratio between the elliptical interpolation perimeter and the perimeter of the actual droplet: an optimal value of 0.875 is found for this criterion. This method is especially useful to exclude the erroneous ligaments for which the large extrapolated diameter is not representative of a real diameter.

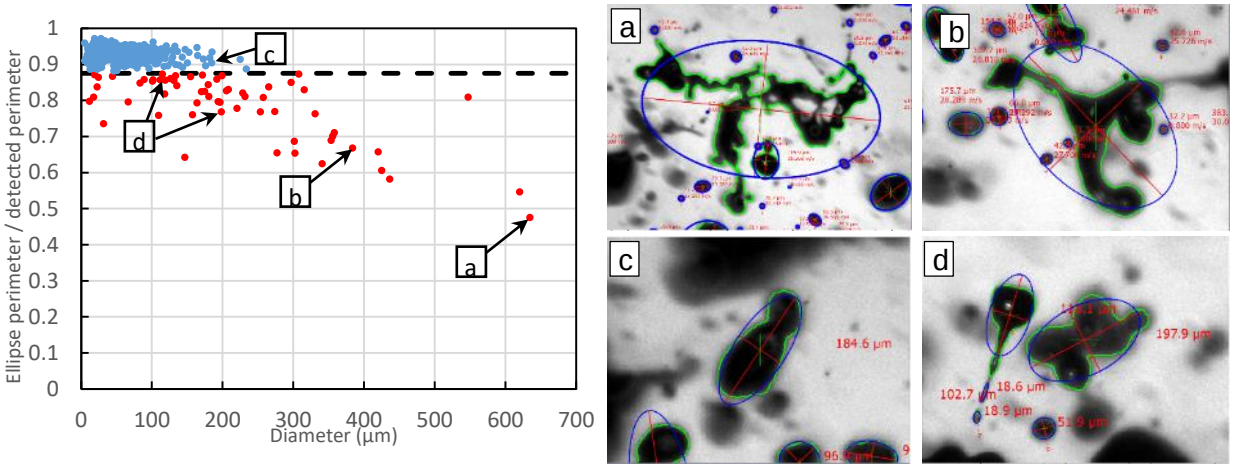

Figure 4. Example of particles excluded (red dots) or included (blue dots) in the statistics. Perimeter detected (green overlay), perimeter of the ellipse (blue overlay). In this case 63 particles are excluded (about 10%) – Water spray, 0.9 MPa, Z/d_0 = 50.

The spray is studied in steady operation. Its wavy behaviour is reported in the literature [2],[6] (see Figure 5 for visualization) and the ligament wavelength is less than 1.0 mm, hence a characteristic frequency about 10 kHz for a typical velocity of 10 m/s. Our diagnostics are compatible with these space and time scales: the shadowgraphy field of view (2.5 x 3.2 mm) corresponds to several wavelengths of the spray (2-3 wavelengths), while PDI is performed over a large number of time-periods (6 kHz in average during 1–2 s). Thus both diagnostics allow a correct sampling.

Besides, the characteristic dimension of the PDI probe volume cross-section (0.34 mm) represents around 10-15% of the shadowgraphy field-of-view. Moreover, shadowgraphy provides uniform results (same drop size distribution and droplet number) whatever the investigation region. Therefore, shadowgraphy and PDI results can be compared in these spray conditions.

Results and discussion

Topology of the spray

The spray is investigated by high-magnification shadowgraphy in the conditions of interest (see Table 1), for water and ethanol. For each spray condition, the measurement point is displaced from the impingement point of the jets, along the spray centreline coordinate Z (see Figure 5). The corresponding shadowgraphy pictures provide an original view of the inner spray structure. Although the topology of such sprays has been thoroughly described in

past studies, the present visualizations offer a detailed description of the primary atomization process (sheet breakup from $Z = 3\ d_0$), and of the secondary atomization process (ligament breakup from $Z = 20\ d_0$). These breakup lengths and wavelengths have been discussed in our previous work concerning like-doublets [6].
Additional information is given by the shape of ligaments and droplets. The dynamics of ligaments has a wavy behaviour that generates elongate blobs and droplets from $Z = 20–30\ d_0$, and these structures exhibit a relaxation process towards a stable shape (i.e. spherical). However, pictures at $Z = 100–150\ d_0$ show that small droplets reach a round shape, whereas the numerous big droplets that remain in the spray still have an elliptical or concave shape. As a result, the biggest droplets may be detected well by shadowgraphy, but hardly by PDI.

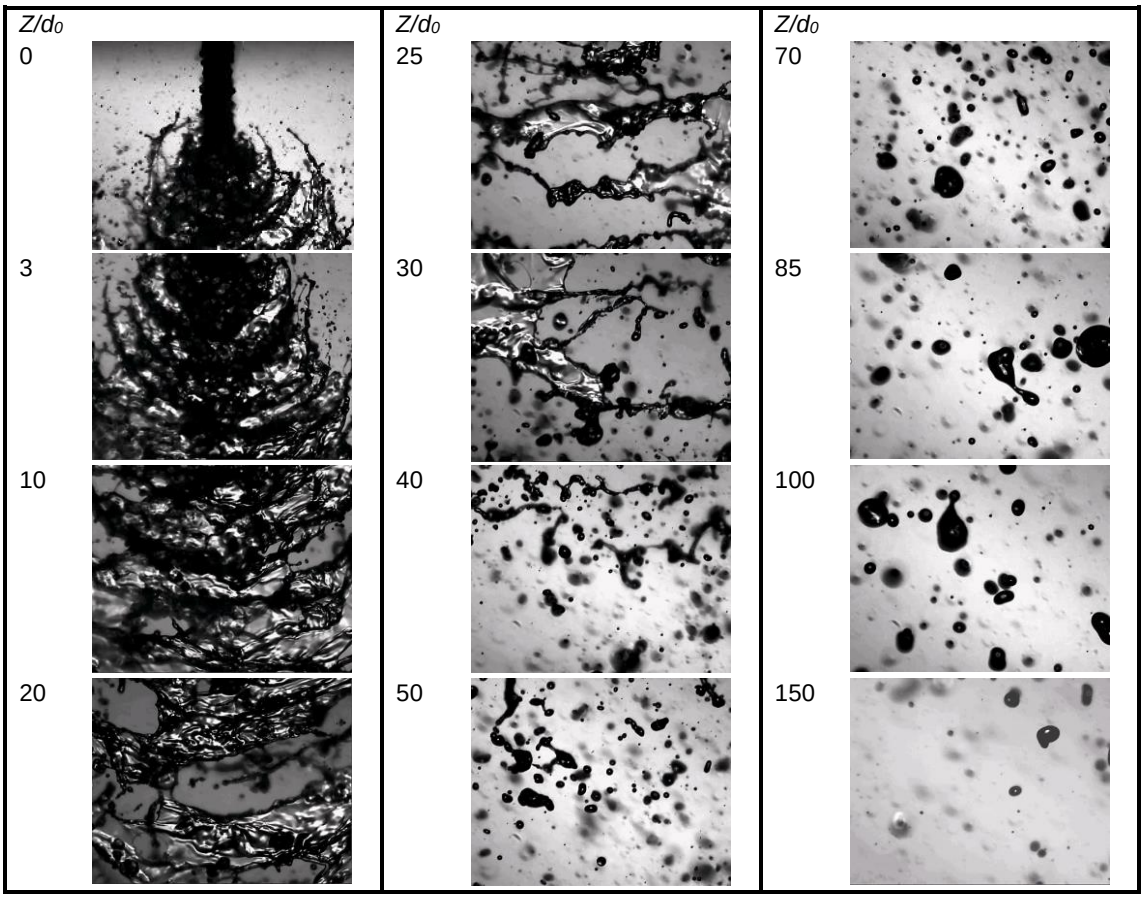

Figure 5. Shadowgraphy of the spray from the impingement point – Water, ΔP = 0.9 MPa, illumination 5 ns, 2.5 x 3.2 mm.

Drop size distributions of the sprays
The above shadowgraphy pictures reveal the structure of the spray as a function of the operating conditions and measurement location. Additional spray pictures highlight the influence of pressure (ΔP) that drives the Reynolds and Weber numbers through jet momentum. As ΔP increases, the spray generates smaller droplets because of this increase in impingement force, which is a common result in like-doublets sprays [2],[5],[7]: this effect is evidenced by PDI and shadowgraphy measurements performed on the same water spray (see Figure 6a).
Both diagnostics show that the drop size distribution is mainly composed of small droplets ($D < 0.20\ d_0$); this is due to the measurement location situated far from the impingement point ($Z/d_0 = 100$) i.e. after secondary breakup. It should be noticed that, in the case of shadowgraphy, the diameter of maximum probability decreases when ΔP increases, while in the case of PDI measurements this diameter is the same but with increasing probability. The same comparison is performed on ethanol spray for the same measurement location, $Z/d_0 = 100$ (see Figure 6b): shadowgraphy and PDI lead to a similar drop size distribution mainly composed of smaller droplets ($D < 0.10\ d_0$) than water distribution. The drop size distribution is smaller for ethanol than for water mainly due to the lower surface tension of ethanol, and subsequently to its higher Weber number (see Table 1). As a conclusion, PDI and shadowgraphy provide similar drop size distributions, with small quantitative differences.
This result is in agreement with comparable work performed on a steady atomizer [9], that also led to quantitative differences between the PDI and shadowgraphy results. A difference was found in the PDF distribution of drop size (albeit normalized in that work [9]), and differences were also reported in the statistical diameters.

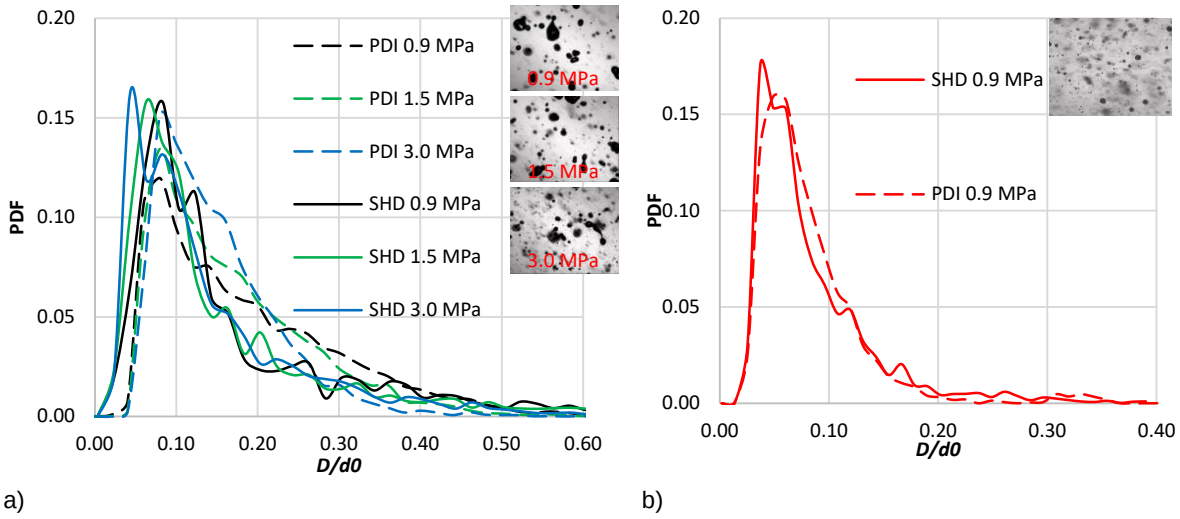

Figure 6. PDF of drop size distribution comparison: a) shadowgraphy vs. PDI, with increasing momentum (water, d_0 = 0.30 mm, Z/d_0 = 100); b) shadowgraphy (d_0 = 0.30 mm) vs. PDI (d_0 = 0.51 mm) – Ethanol, Z/d_0 = 170, ΔP = 0.9 MPa.

Effect of distance from the impingement point

The evolution of this distribution is investigated at different measurement locations by shadowgraphy (see Figure 7a): as distance Z increases from the impingement point, the distribution exhibits droplets of smaller size ($D < 0.05\ d_0$). And yet, as Z increases, the characteristic diameter computed from the drop size distribution has distinct behaviours in other work: SMD increases [5]-[6] or decreases [3] with increasing distance from the impingement point. Therefore, a characteristic diameter should be evaluated to quantify this effect. For this purpose, the average diameter *D10* is chosen because it represents fairly the whole drop size distribution, taking care to the geometrical drop size that is detected directly by shadowgraphy.

The average diameter *D10* is computed from PDI and shadowgraphy measurements on ethanol and water sprays at ΔP = 0.9 MPa (see Figure 7b). The *D10* computed with shadowgraphy is roughly constant for water, and decreases slightly with increasing distance Z in the case of ethanol. The *D10* for water measured with PDI is higher, which is consistent with the drop size distribution (see Figure 7a), and decreases slightly with increasing distance Z, while the validation rate of the PDI instrument increases up to 80%. In the meantime, the corresponding shadowgraphy pictures (see Figure 5) demonstrate that water droplets turn overall from ligaments and concave droplets (Z/d_0 = 50), to convex droplets (Z/d_0 = 150) which cross-section is not perfectly circular. This may explain the difference between the PDI measurement, that is based on the spherical assumption, and the shadowgraphy measurement that encompasses any droplet shape.

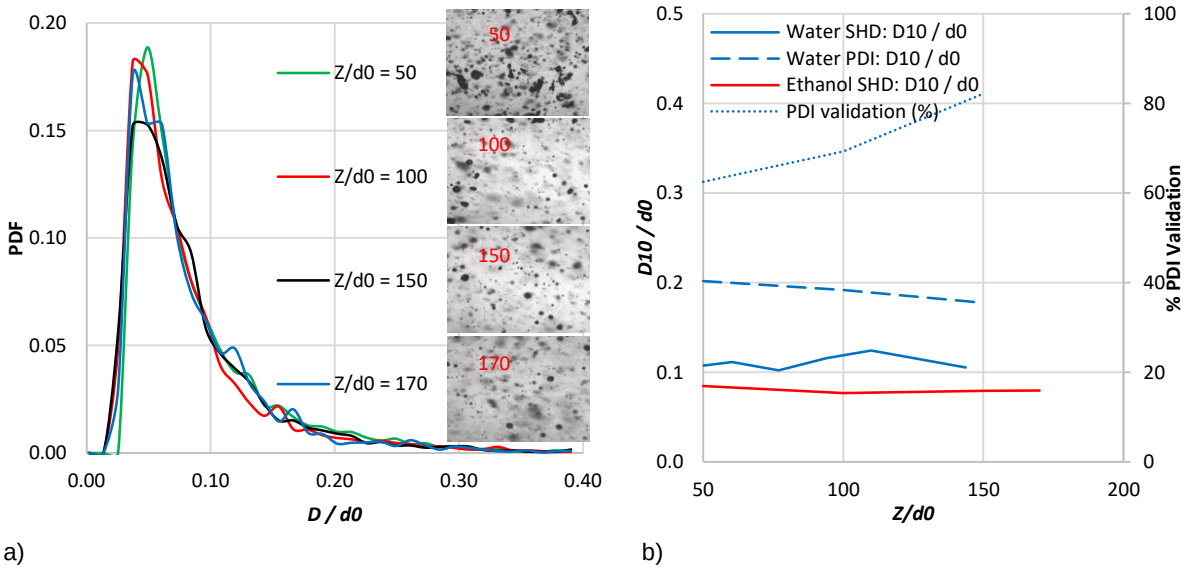

Figure 7. Effect of distance Z from the impingement point (d_0 = 0.30 mm, ΔP = 0.9 MPa): a) PDF of ethanol drop size distribution by shadowgraphy; b) average diameter *D10* computed from PDI or shadowgraphy.

Distribution of droplet shapes

From the above comparison, we can assume that the shadowgraphy measurements are less restrictive than PDI, as far as droplet shape is concerned. In order to confirm this assumption, the droplet shapes detected by the abovementioned shadowgraphy method are further analysed. For this, the centricity distribution of elliptical droplets cross-section is reported for water and ethanol sprays at Z/d_0 = 50 and 150, ΔP = 0.9 MPa (see Figure 8a); the ellipse centricity is defined as the ratio of its short axis to long axis. For both fluids, the centricity distribution is closer to unity in the dilute spray region (Z/d_0 = 150) than in the dense region (Z/d_0 = 50), thus confirming that some time is required after breakup to generate round droplets. In contrast, the PDI diagnostic may detect only the droplets of centricity close to unity. This causes a bias in the spray characterization because droplets of centricity lower than 0.80 still represent a significant part of the distribution in our case: 10–20% in the dilute spray (Z/d_0 = 150), but 30–40% in the dense region (Z/d_0 = 50). It is necessary to assess which class of diameter is affected by this bias.

The centricity of maximum probability is reported for each class of diameter, for water and ethanol sprays at Z/d_0 = 150, ΔP = 0.9 MPa (see Figure 8b); the velocity associated to each droplet is also reported. Most spherical droplets (of centricity close to 1) can be found in the range of diameter 30–100 µm, while the other droplets are of lesser centricity. The smallest droplets (D < 30 µm) are less spherical, and their velocity is much lower than bigger droplets. This may be due to the effect of the aerodynamic drag, that affects significantly this class of small droplets. Under this effect, the unstable droplet shape oscillates due to the surface tension that tends to restore its round shape, hence a periodic, elliptic deformation [10]. The biggest, elongate elliptical droplets (D > 100 µm) may proceed from ligament parts (see Figure 8a). These large elliptical droplets may be difficult to probe with PDI considering the stringent tolerance in the maximum phase difference between pairs of detectors, but they carry a significant amount of liquid with poor evaporation surface. Consequently, they deserve appropriate diagnostics such as shadowgraphy. Their importance is superior in the dense region (Z/d_0 = 50); downstream, in the dilute region (Z/d_0 = 150), largest droplets seem to relax towards spherical shape.

This effect is observed either on water or ethanol, but ethanol seems to produce more elliptical droplets. This is consistent with its lower surface tension compared to water, hence a higher sensitivity to initial conditions (ligament breakup) and a lesser cohesion prone to the oscillating deformation of ethanol droplet.

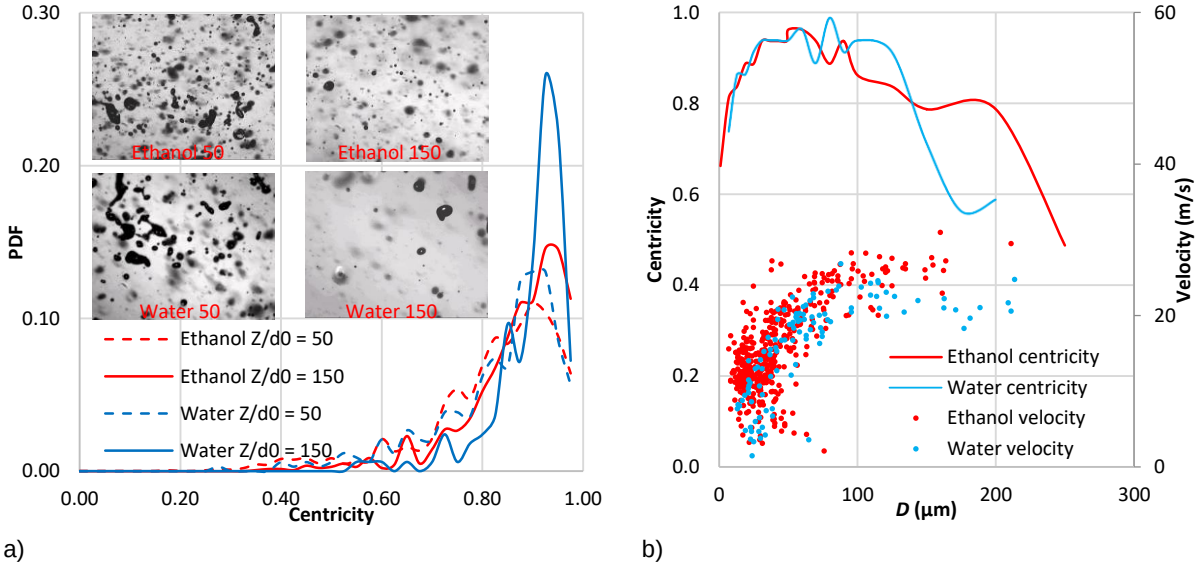

Figure 8. Centricity of elliptical droplets computed from shadowgraphy pictures of water and ethanol sprays (d_0 = 0.30 mm, ΔP = 0.9 MPa): a) distribution of centricity; b) evolution of centricity and velocity vs. droplet diameter at Z/d_0 = 150.

Conclusions

This study demonstrates the interest of high-magnification shadowgraphy for the study of impinging jet injector. It allows to visualize directly the atomization process, and proves to be particularly useful for direct measurements of drop size, velocity and shape inside dense sprays. Indeed, this atomization process generates various shapes of drops and ligaments, especially non-spherical droplets, most of which can be detected by an elliptical interpolation. It is noticeable that most of the largest droplets generated by this injector are characterized by an elliptical shape, and consequently may be rejected by PDI.

In the present study, shadowgraphy provides original data concerning the spray topology, as well as droplet morphology, diameter and velocity. The distribution of droplet size has been recorded along the spray centreline, highlighting the effect of jet momentum (driven by injection pressure) and the evolution versus distance from the impingement point. Overall, it is clear that ethanol is prone to generate quickly smaller droplets sprays than water (thus hydrogen peroxide), thanks to its lower surface tension. This effect is quantified clearly by the drop size distributions and mean droplet diameters.
The fluids investigated in this work stand for green storable bi-propellants, such as ethanol (fuel) and hydrogen peroxide (represented by water). Experimental conditions led to ligament- or fully-developed breakup atomization regimes, representative of some engine injector conditions. As far as engine combustion is concerned, the elevated pressure and temperature conditions may modify the spray structure, and combustion may interact with the spray so that the evaporation time allowed to the propellants is limited. In this context, the influence of large droplets is paramount and should be taken into account from the injector characterization.

Acknowledgements
The authors wish to acknowledge the support of CNES (French Space Agency).

Nomenclature

ΔP	Pressure drop across the injector [MPa]
μ	Dynamic viscosity [kg/m/s]
ρ	Liquid density [kg/m^3]
σ	Surface tension ([N/m]
d_0	Nozzle diameter [mm]
D	Droplet diameter [µm]
$D10$	Mean droplet diameter [µm]
Oh	Ohnesorge number
PDF	Probability Density Function
PDI	Phase-Doppler Interferometer
Re	Reynolds number
SMD	Sauter Mean Diameter [µm]
V	Liquid jet velocity [m/s]
We	Weber number
Z	Distance along the spray centreline [mm]

References

[1] Bailardi, G., Negri, M. and Ciezki, H. K., “Several aspects of the atomization behavior of various newtonian fluids with a like-on-like impinging jet injector”, ILASS-Europe 2010, 23rd Annual Conference on Liquid Atomization and Spray Systems, Brno, Czech Republic, 2010.
[2] Ryan, H. M., Anderson, W. E. and Pal, S., “Atomization characteristics of impinging liquid jets”, J. of Propulsion and Power, 11 (1), pp. 135-145, 1995.
[3] Zheng, G., Nie, W., Feng, S., Wu, G., "Numerical simulation of the atomization process of a like-doublet impinging rocket injector", Procedia Engineering 99, pp. 930-938, 2015.
[4] Chen, X., Ma, D., Yang, V., Popinet, S., "High-fidelity simulations of impinging jet atomization", Atomization and Sprays, 23 (12), pp. 1079–1101, 2013.
[5] Sakisaka, R., Hayashi, J., Daimon, Y, Yamanishi, N., Akamatsu, F., "Experimental measurements of impinging jet atomization at the vicinity of liquid fan", ICLASS 2012, 12th Triennial International Conference on Liquid Atomization and Spray Systems, Sep. 2-6, 2012.
[6] Indiana, C., Bellenoue, M., Boust, B., "Experimental investigations of drop size distributions with impinging liquid jets using phase-Doppler anemometer”, International Journal of Energetic Materials and Chemical Propulsion 14 (3), pp. 241-264, 2015.
[7] Ramamurthi, K., Nandakumar, K. and Patnaik, R. K., “Characteristics of sprays formed by impingement of a pair of liquid jets”, J. of Propulsion and Power, 20 (1), pp. 76-82, 2004.
[8] Indiana, C., Bellenoue, M., Boust, B., Petitot, S., “Experimental combustion investigations from like-impingement sprays of green propellants”, 52nd AIAA/SAE/ASEE Joint Propulsion Conference, Salt Lake City (USA), 25-27 July 2016.
[9] Berg, T., Deppe, J., Michaelis, D., Voges, H., Wissel, S., "Comparison of particle size and velocity investigations in sprays carried out by means of different measurement techniques", ICLASS 2006, International Conference on Liquid Atomization and Spray Systems, Aug. 27 - Sep. 1, 2006.
[10] Suh, Y., Lee, C., "A numerical method for the calculation of drag and lift of a deformable droplet in shear flow", Journal of Computational Physics 241 (15) pp. 35–57, 2013.